

*Annual Review of Fluid Mechanics*

# Vortices and Forces in Biological Flight: Insects, Birds, and Bats

Hao Liu,<sup>1</sup> Shizhao Wang,<sup>2</sup> and Tianshu Liu<sup>3</sup>

<sup>1</sup>Graduate School of Engineering, Chiba University, Chiba, Japan; email: hliu@faculty.chiba-u.jp

<sup>2</sup>State Key Laboratory of Nonlinear Mechanics, Institute of Mechanics, Chinese Academy of Sciences, Beijing, People's Republic of China; email: wangsz@lnm.imech.ac.cn

<sup>3</sup>Department of Mechanical and Aerospace Engineering, Western Michigan University, Kalamazoo, Michigan, USA; email: tianshu.liu@wmich.edu

Annu. Rev. Fluid Mech. 2024. 56:147–70

First published as a Review in Advance on  
September 22, 2023

The *Annual Review of Fluid Mechanics* is online at  
fluid.annualreviews.org

<https://doi.org/10.1146/annurev-fluid-120821-032304>

Copyright © 2024 by the author(s). This work is licensed under a Creative Commons Attribution 4.0 International License, which permits unrestricted use, distribution, and reproduction in any medium, provided the original author and source are credited. See credit lines of images or other third-party material in this article for license information.

ANNUAL  
REVIEWS **CONNECT**

[www.annualreviews.org](http://www.annualreviews.org)

- Download figures
- Navigate cited references
- Keyword search
- Explore related articles
- Share via email or social media

## Keywords

biological flight, flapping wing, vortex dynamics, unsteady aerodynamics, modeling

## Abstract

Insects, birds, and bats that power and control flight by flapping their wings perform excellent flight stability and maneuverability by rapidly and continuously varying their wing motions. This article provides an overview of the state of the art of vortex-dominated, unsteady flapping aerodynamics from the viewpoint of diversity and uniformity associated with dominant vortices, particularly of the relevant physical aspects of the flight of insects and vertebrates in the low- and intermediate-Reynolds-number ( $Re$ ) regime of  $10^0$  to  $10^6$ . After briefly describing wing morphology and kinematics, we discuss the main vortices generated by flapping wings and the aerodynamic forces associated with these structures, focusing on leading-edge vortices (LEVs), wake vortices, and vortices generated by wing motions over a broad  $Re$  range. The LEVs are intensified by dynamic wing morphing in bird and bat flight, producing a significantly elevated vortex lift. The complex wake vortices are the footprints of lift generation; thus, the time-averaged vortex lift can be estimated from wake velocity data. Computational fluid dynamics modeling, quasi-steady models, and vortex lift models are useful tools to elucidate the intrinsic relationships between the lift and the dominant vortices in the near- and far-fields in flapping flight.

## 1. INTRODUCTION

Over a long evolutionary period, natural flyers (insects, birds, and bats) have achieved excellent flight performance for their survival in specific environments by flapping their wings in a broad-Reynolds-number ( $Re$ ) range ( $10^0$ – $10^6$ ) (Sane 2003, Liu et al. 2016). Although wing shape, size, weight, and kinematics of insects, birds, and bats vary considerably in scale (**Figure 1a**), vortex-dominated unsteady flows are the essential physical aspect of biological flight. The central challenge is to unveil the sophisticated mechanisms by which natural flyers achieve diverse but robust flapping flight with complex dynamic wing morphologies while coping with complex environments.

The unsteady flows in biological flapping flight are dominated by various near- and far-field large-scale coherent vortices with complicated topology. For example, the prominent vortices associated with hawk moth hovering flight are illustrated in **Figure 1b**. A horseshoe-shaped vortex (HSV) is initially generated in early downstrokes and upstrokes; it wraps around each wing and comprises a leading-edge vortex (LEV), a wing tip vortex (TV), and a trailing-edge vortex (TEV), substantially forming a vortex sheet that rolls into a series of vortices. The HSV grows into a vortex ring (VR), inducing a jet-stream downwash in its core, that eventually breaks up into two or more smaller VRs in the wake. **Figure 1c** shows the complex near- and far-field vortices of a hawk moth in forward flapping flight. For flapping bat wings, the LEVs and TVs are the main features. The stable LEV is widely accepted as the universal unsteady aerodynamic mechanism responsible for augmenting lift production in flapping flight observed at all  $Re$  (or sizes) for insects, birds, and bats (Chen & Lentink 2016, Liu et al. 2016). In the intermediate- $Re$  regime of bat and bird flight, more complex flow structures are associated with laminar-turbulent flow transition and turbulent flows generated by complex dynamic wing morphologies (**Figure 1d**). Moreover, the wings of these flyers have joints and/or flexible structures that have chordwise, spanwise, and twist deformation during flapping flight, which can actively and/or passively control the LEVs and the unsteady lift. Additionally, fast flapping wings in insects and morphing wings in bats and birds are more resistant to wind gusts and freestream turbulence, implying that the vortex-dominated unsteady aerodynamics in biological flight is likely highly robust.

Due to the complexity and nonlinearity of the vortex-dominated flow structures associated with natural flyers, it is generally acknowledged that conventional aerodynamics models are not sufficient to explain how these flyers achieve high lift in flapping flights. Researchers have proposed various lift-enhancing mechanisms, such as the LEV-based delayed stall, clap and fling, rotational circulation, wake capture, and dynamically changing wingspan. Considerable effort to understand the unsteady vortices and aerodynamic forces in flapping flight has been made through computational fluid dynamics (CFD), experiments in wind tunnels, and field measurements. Since the physical aspects of biological flapping flight are diverse and existing results are fragmental, it is desirable to examine the vortex-dominated unsteady aerodynamics from a more unified viewpoint, focusing on near- and far-field vortices and relevant unsteady force generation.

Several review articles on specific aspects of this topic deal with insect flight (Wang 2005), theoretical models of fish swimming and bird and insect flight (Wu 2011), the LEVs at low  $Re$  (Eldredge & Jones 2019), and aeroacoustics of owl flight (Jaworski & Peake 2020). Here, we attempt to elucidate the vortex-dominated flow physics associated with flapping flight, focusing on the relationships between unsteady vortices and aerodynamic forces by examining computational and experimental results and evaluating relevant aerodynamic models. We discuss the main technical aspects, such as the LEVs, interplay between the LEVs and the TVs, wing–body interaction, deformation-/morphing-induced wing–flow interaction, and wing–wake interaction, from a combined theoretical, computational, and experimental perspective. Furthermore, we assess

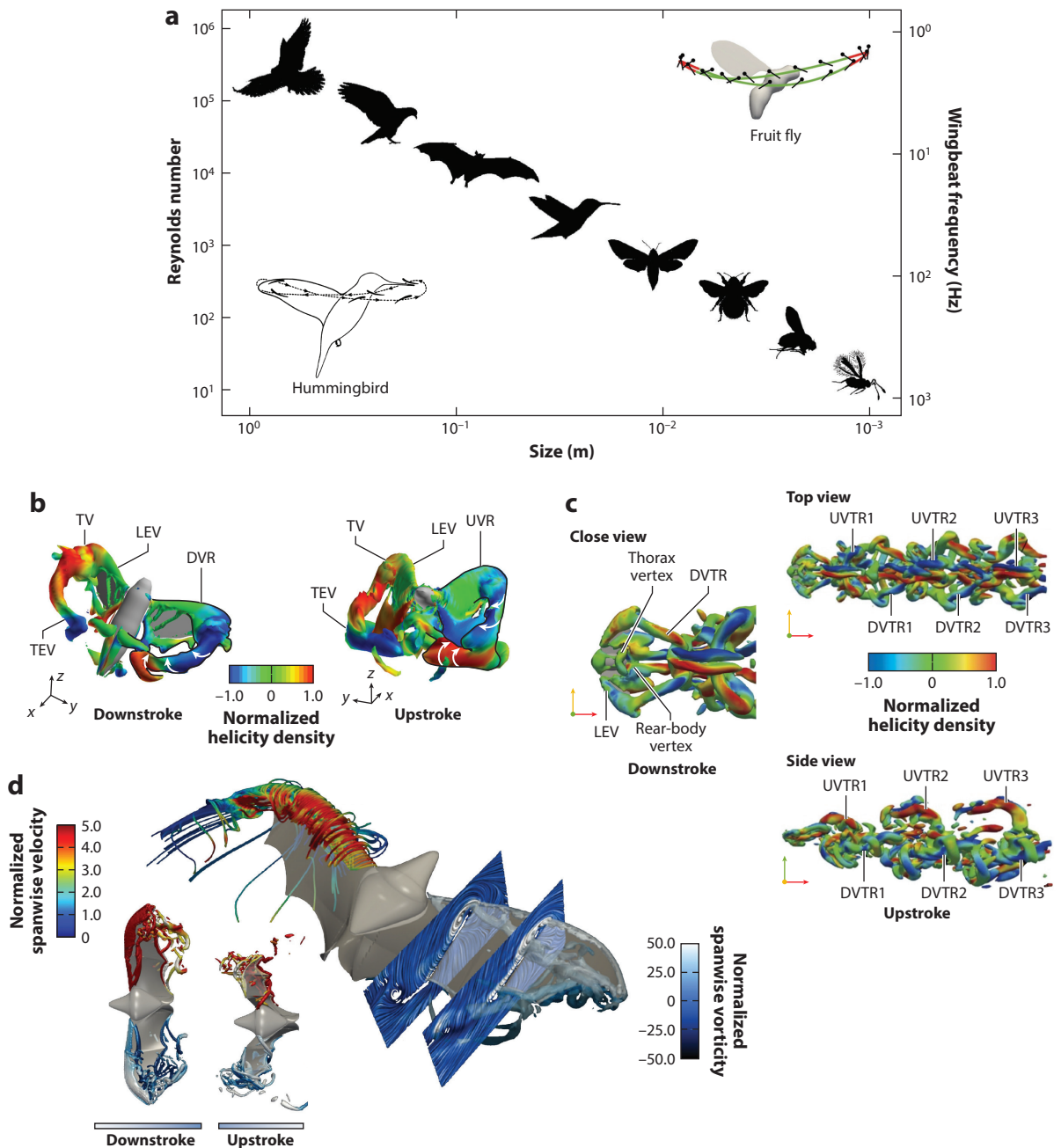


**Figure 1**

(a) Prominent wing morphologies, sizes, Reynolds numbers, and wingbeat frequencies in biological flapping flight. (b) Near- and far-field vortices (Q-surfaces, where Q is the second invariant of the strain rate tensor) in hawk moth hovering. Panel adapted from Liu (2009). (c) Wake topologies (Q-surfaces) in hawk moth forward flight at a speed of 3.8 m/s. Panel adapted from Xue et al. (2022). (d) Vortices and wing morphology of a slow-flying bat. Panel adapted from Wang et al. (2015a). Abbreviations: DVR, downstroke vortex ring; DVTR, downstroke vortex-tube ring; LEV, leading-edge vortex; TEV, trailing-edge vortex; TV, wing tip vortex; UVR, upstroke vortex ring; UVTR, upstroke vortex-tube ring.

aerodynamic models such as lift decomposition, wake models, quasi-steady models, CFD-based models, and CFD data-driven models, focusing on the validity and accuracy in modeling and predicting the unsteady aerodynamic forces. Finally, we summarize the main results and the future issues in the field.

## 2. WING MORPHOLOGY AND WING KINEMATICS

### 2.1. Wing Morphology

Wing morphology in flying insects (**Figure 1a**) is normally characterized by a very thin plate with a low-aspect ratio (AR) planform (Xu et al. 2021). Such a flat, platelike wing has an extremely low wing-to-body mass ratio, less than 1% for most flying insects, which can significantly reduce inertial forces and achieve fast wing-stroke motions. The wing geometry of birds is normally determined by airfoil sections and the wing planform projected onto the level plane. Bird airfoil is characterized by the mean camber line and thickness distribution (Nachtigall & Wieser 1966, Liu et al. 2006, Carruthers et al. 2010). Bats have membranous wings stretched by elongated forelimb bones and modified hindlimb bones with more than 20 joints (Amador et al. 2020), exhibiting an ability to control the wing planform and airfoil camber to meet flight demands. The wing of a bird or bat is usually divided into an arm-wing (inner wing between the shoulder and the wrist) and a hand-wing (outer wing between the wing tip and the wrist).

### 2.2. Wing Kinematics

Wing kinematics in insect flapping flight can be described by three Eulerian angles with respect to the stroke plane: the positional angle ( $\phi$ ), the elevation angle ( $\theta$ ), and the feathering angle ( $\alpha$ ) (**Figure 2**). For a hovering flyer these angles can be expressed with the Fourier series in terms of the geometric angle of attack (AoA) of a wing, which can be determined from the measured kinematic data (Liu et al. 1998, Liu 2009). The body kinematics can be characterized by the body angle ( $\chi$ ) and the stroke plane angle ( $\beta$ ), depending on flight speed. The flapping motion of insect wings has two phases: translation during the front and back strokes and rotation in the transitions between strokes (**Figures 1a** and **2a**). The wing-stroke motion in insect flight is actuated by a complex musculoskeletal system with a flexible wing hinge that passively alters the wing kinematics and aerodynamics (Liu 2020). Thus, flapping-wing dynamics is determined by the interplay among wing inertia, aerodynamics, and wing-hinge mechanics (Beatus & Cohen 2015).

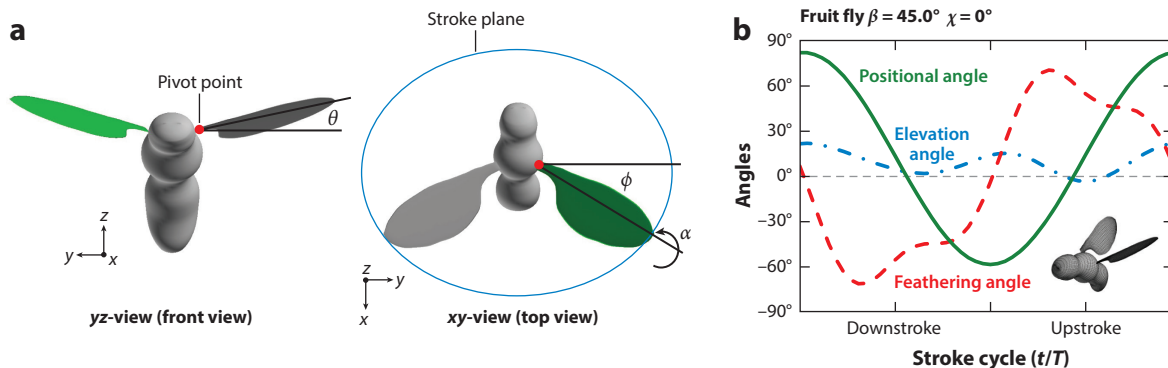


**Figure 2**

Flapping insect wing kinematics. (a) Schematic of three Eulerian angles, positional ( $\phi$ ), feathering ( $\alpha$ ), and elevation ( $\theta$ ), of wing-stroke motion. (b) The stroke plane angle ( $\beta$ ) and the body angle ( $\chi$ ) in fruit fly hovering. Figure adapted from Liu & Aono (2009).

A flapping bird wing changes the wing planform, area, twist, and bending between upstrokes and downstrokes. The wing kinematics, including the heaving motion, dynamically changing wingspan, and sweeping hand-wing, was determined from high-speed videos of flying birds (owl, seagull, crane, and goose) (Liu et al. 2006, Wolf & Konrath 2015). Once the wing geometry (airfoil sections, planform, and twist distribution) and the kinematics of the quarter-chord line of a wing are given, a flapping wing can be reconstructed (Liu et al. 2006).

The kinematics of a bat wing was measured and reconstructed with the proper orthogonal decomposition (Riskin et al. 2008, Viswanath et al. 2014) and the Gaussian process dynamic model (Bender et al. 2019). Flapping bat wings stretch in downstroke and retract toward the body in upstroke, resulting in a dynamically changing wingspan. The span ratio between the minimum and the maximum wingspans is introduced to measure the magnitude of the stretching and retracting wingspan. The span ratio of bat wings is approximately 0.6 at the lowest speed and 0.70–0.75 at medium and high speeds, which is higher than that for most birds (Norberg & Winter 2006, Tobalske 2007). For further details on bat wing morphology and kinematics, we refer the reader to Hedenström & Johansson (2015), Swartz & Konow (2015), Amador et al. (2020), and Sadier et al. (2020).

### 3. VORTICES OF FLAPPING WINGS

#### 3.1. Leading-Edge Vortex

The LEV, which is observed at all  $Re$  (or sizes) for insects, birds, and bats (Chen & Lentink 2016, Liu et al. 2016), is stable and robust and widely accepted as the universal unsteady aerodynamic mechanism responsible for augmenting lift production in flapping flight.

**3.1.1. Observations of leading-edge vortices.** The LEV is a convergent and robust mechanism normally observed in a large  $Re$  range (sizes) in the translation stroke of flapping wings (**Figure 1**) of insects (Ellington et al. 1996, Bomphrey et al. 2005), birds (Videler et al. 2004; Warrick et al. 2005, 2012; Hedenström et al. 2007, 2009; Muir et al. 2017), and bats (Muijres et al. 2008, Hedenström & Johansson 2015) that prevents stall at high AoAs and augments lift production. The LEVs of flapping wings have been identified in experiments using dynamically scaled mechanical models (van den Berg & Ellington 1997, Lu et al. 2006, Lentink & Dickinson 2009, Phillips et al. 2015) and in CFD simulations (Liu et al. 1998, Sun & Wu 2003, Liu 2009, Liu & Aono 2009, Song et al. 2014) of various realistic and simplified models with flapping or revolving kinematic protocols (Kim & Gharib 2010, Ozen & Rockwell 2012, Garmann & Visbal 2014, Harbig et al. 2014, Carr et al. 2015, Wolfinger & Rockwell 2015).

In insect flapping flight in the low- $Re$  regime ( $<10^4$ ), as the wing translates during the downstroke and upstroke at high AoAs (**Figure 2**), the flow separates from the leading edge, forming an intense and stable vortex that persists above the suction side of the wing during most of the wingbeat stroke (**Figure 3**). The pressure deficit in the vortex core produces a triangular low-pressure region that extends to the wing tip near the leading edge (Chen et al. 2017b). The main characteristics and implications of the LEV on the lift generation varied with changes in the  $Re$ , the reduced frequency ( $k$ ), the Strouhal number ( $St$ ), the wing flexibility, and the wing kinematics. For instance, the LEV structure varies remarkably, from a diffuse vortex with a moderate spanwise flow in fruit fly hovering (**Figure 3b**) at an  $Re$  of 100 to 200 (Lentink & Dickinson 2009; Harbig et al. 2014, 2013) to a conically compact vortex with a characteristic spiral axial flow in bumble bee hovering (**Figure 3c**) when  $Re$  exceeds 1,000 (Liu 2009, Garmann & Visbal 2014, Carr et al. 2015).

Compared with our understanding of insect flight, results for near- and far-field vortex dynamics in bird and bat flight are limited due to the morphological complexity and dynamic variation of

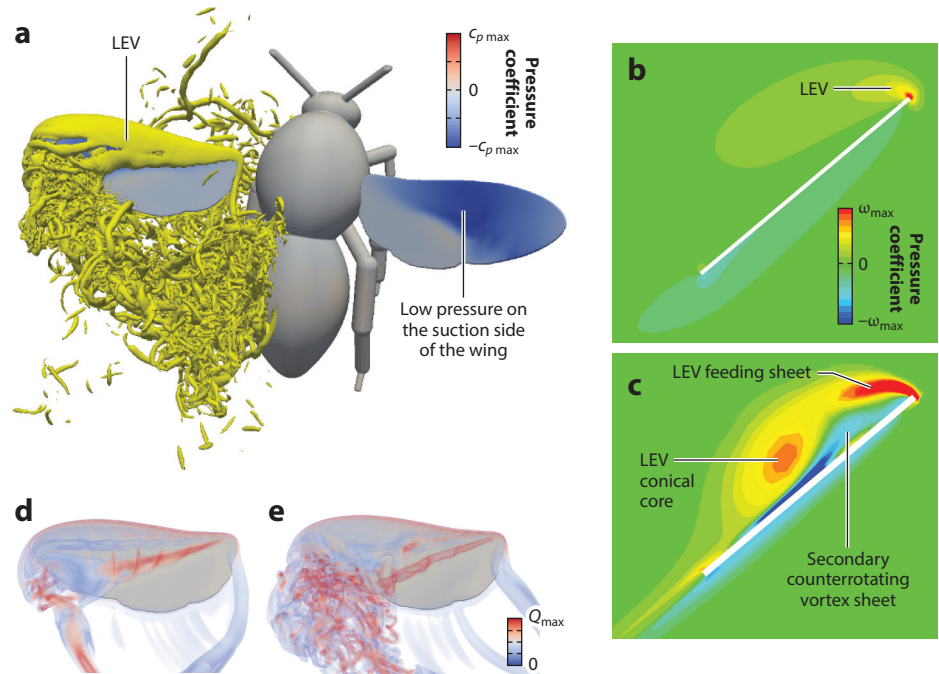


**Figure 3**

The leading-edge vortices (LEVs) over flapping and revolving wings of a hovering bumble bee. (a) LEV and surface pressure distribution on a flapping wing. (b,c) Sectional plots of the spanwise vorticity component of a revolving fruit fly wing at Reynolds number ( $Re$ ) = 100 and a revolving bumble bee wing at  $Re = 2,100$ . (d,e) Visualized Q-surface of the flow over a revolving bumble bee wing at the onset of the LEV breakdown (rotational angle  $\varphi = 81^\circ$ ) and long after the LEV breakdown ( $\varphi = 138^\circ$ ) at  $Re = 3,000$ . Figure adapted from Liu et al. (2017).

their wings (Chen & Lentink 2016). Nevertheless, at higher  $Re$  of birds and bats, the LEVs have also been identified as a convergent structure in the flapping flight of birds' and bats' dynamically changing planform (i.e., a morphing wing) (Videler et al. 2004, Lentink et al. 2007, Muijres et al. 2008). A stable LEV was also observed on a mechanical bat wing in experiments (Koekkoek et al. 2012). The LEVs that intensified dynamic wing morphing were investigated with numerical simulations (Wang et al. 2014, 2022). In addition, Linehan & Mohseni (2020) inferred that the LEV over a bird's hand-wing was induced by the alula, enhancing the lift when maneuvering at slow speeds.

The LEV can be stabilized by the spanwise pressure gradient, centripetal force, and Coriolis force induced by the wing revolving/rotating and wing acceleration, driving the axial flow along the wingspan, depending on the sizing effect and wing kinematics (Ozen & Rockwell 2012, Liu et al. 2017). The stability of the LEV is affected by several mechanisms: von Kármán–vortex-type shedding instability, Kelvin–Helmholtz (KH) instability, vortex breakdown, and Coriolis force.

**3.1.2. von Kármán–vortex-type shedding instability.** The spanwise flow generated by the wing-rotation-driven centripetal force (proportional to the radial position) in flapping and revolving wings, which are different from unilaterally translating wings, can stabilize the LEV, dominating the growth of the vortex core and its spanwise convection toward the wing tip (Figures 3d,e). CFD and experimental studies indicate that to avoid the LEV shedding from a revolving wing, the chord length should be larger than the vortex size at the same location

(Kolomenskiy et al. 2014, Kruyt et al. 2015, Phillips et al. 2015, Chen et al. 2017a). The LEV shedding instability is less sensitive to AoA between 30° and 90°, where similar conical LEVs are produced (Garmann & Visbal 2014) when the ratio of the wingspan to the chord length is less than 3 or 4 (Wolfinger & Rockwell 2014, Carr et al. 2015).

**3.1.3. Kelvin–Helmholtz instability.** When the  $Re$  is sufficiently high ( $>10^3$ ) for a large-AR wing, such that the feeding vorticity sheet of the arch-like LEV is sufficiently thin, KH instability occurs (Garmann & Visbal 2014). The resulting shear-layer substructures form dual LEV cores (Lu et al. 2006) (**Figure 3c**), and such topological transition is suggested to be controlled by span-based  $Re$  (Harbig et al. 2013, Carr et al. 2015). However, KH instability has a small influence on LEV-induced force production (Garmann & Visbal 2014, Engels et al. 2016).

**3.1.4. Vortex breakdown.** The LEV breakdown that occurs in helical vortices normally shows a large axial pressure gradient (Liu et al. 1998, Maxworthy 2007, Liu 2009). Once the conical LEV is formed, the centrifugal force creates a strong spanwise pressure gradient, which enhances the axial velocity in the vortex core. As observed in hawk moth and bumble bee hovering, the LEV bursts at 70–90% of the wingspan when the vortex core increases sufficiently to form a large bubble-like structure while the spanwise pressure gradient and a TV-induced opposite pressure gradient become unbalanced (Liu et al. 1998, Shyy et al. 2010). The vortex breakdown has less impact on the production of aerodynamic force (Garmann & Visbal 2014, Engels et al. 2016). Even in the turbulent environment, the LEVs do not lose their coherence, and the mean vertical aerodynamic force remains invariant regardless of the turbulence intensity (Engels et al. 2016).

**3.1.5. Role of Coriolis force.** In the reference frame rotating with the wing, the azimuthal and radial components of the Coriolis force are nonzero, and its prevailing direction points from the wing surface toward the wake and inward to the rotational axis (Garmann & Visbal 2014). While the Coriolis force shows a destabilizing effect by curving the neutral streamline toward the trailing edge and hence approaching the vortex shedding (Limacher et al. 2016), the LEV was featured and stabilized (Jardin & David 2015) owing to the combined effect of the centrifugal and Coriolis accelerations induced by the wing rotation characterized by the Rossby number (Chen & Lentink 2016).

## 3.2. Vortices During Wing Rotation

Vortices were also observed during wing rotation of the wingbeat stroke (**Figures 1 and 3**) (Weis-Fogh 1973, Dickinson et al. 1999) and can be classified as resulting from the Framer effect, clap-and-fling mechanism, or wing–wake interaction.

**3.2.1. Framer effect.** The Framer effect is observed during pronation and supination of wing rotation, producing additional circulation so that the flows over both wing surfaces join smoothly at the trailing edge. This leads to the augmented lift during the translation stroke in terms of advanced rotation and delayed rotation (Dickinson et al. 1999, Sane 2003), further optimizing flight efficiency with symmetric rotation through a combination of rotation timing and duration (Chen & Lentink 2016).

**3.2.2. Clap and fling.** During pronation, the clap-and-fling mechanism can enhance lift through interactions between paired flapping wings, which was originally observed in a chalcid wasp and later in numerous insects such as hawk moths, butterflies, fruit flies and other dipterans,

wasps, and thrips (Weis-Fogh 1973, Brodsky 1991, Srygley & Thomas 2002). This mechanism is observed during more demanding flight behaviors such as carrying loads and making sharp turns and during takeoff and climbing flight (Wakeling & Ellington 1997).

Three unsteady processes are clarified: (a) the flap-induced mechanism, in which circulation and lift can be enhanced owing to a leading-edge-based fast rotation while producing thrust; (b) the fling-induced mechanism, in which a rapidly developed LEV owing to the opening of the wings and a fast trailing edge-based rotation can swiftly generate the bound circulation and low pressure near the leading edges, enhancing lift; and (c) the clap, which maximizes stroke amplitude, substantially increasing the aerodynamic forces (Sane 2003). The clap-and-fling motion has been studied theoretically (Lighthill 1975), experimentally (Lehmann & Pick 2007), and computationally (Liu & Aono 2009, Miller & Peskin 2009, Santhanakrishnan et al. 2014).

**3.2.3. Wing-wake interaction.** During stroke reversal, the wing can capture vortices that were shed during the previous stroke due to the wing-wake interaction (Dickinson et al. 1999, Birch & Dickinson 2003). This wake capture was observed with a dynamically scaled robotic model of a fruit fly wing (Lehmann et al. 2005), which showed an increase in the effective flow velocity relevant to the wing, generating a peak in force immediately after wing reversal. This unsteady aerodynamic effect has been explained as a result of wake capture (Dickinson et al. 1999), the added-mass effect (Sun & Tang 2002), and the impulsive-start effect associated with the acceleration of the wing (Liu 2009).

The wing-wake interaction is also observed in the TV and TEV. As shown in **Figure 1b**, the LEV, TV, and TEV form a VR during the translation, resulting in the wing-wake interaction and thus augmenting force production. The TVs in a flapping wing can either promote or have little effect on the aerodynamics of a low-AR flapping wing in some specific kinematic motions (Shyy et al. 2009). Particle image velocimetry (PIV) measurements and CFD simulations showed that mosquitoes in free flight, with high-AR wings flapping at high frequencies ( $>800$  Hz) and stroke amplitudes lower than those of any other insect group, utilized the TEVs caused by wake capture at stroke reversal and rotational drag to enhance force production (Bomphrey et al. 2018). In forward flight, insects benefit from the wing-body-wake interaction in terms of the body vortex, augmenting lift production particularly at fast flights (e.g., a 10% increase in hawk moth forward flight) (Yao & Ye 2020, Xue et al. 2022).

### 3.3. Vortices in Bristled Wings

Very small insects with a body length less than 1 mm (such as wasps and thrips) have bristled wings that comprise a wing pad and numerous high-AR bristles on the fringes (**Figure 4a**). The bristled wings exhibit novel flight performance while challenging the aerodynamic limitations in low-speed flow regimes (Sane 2016, Farisenkov et al. 2020). Compared with large insects with membranous wings, very small insects normally fly at  $Re < 40$ , with U-shaped wing kinematics (Lyu et al. 2019), enabling the drag-based mechanisms that produce sufficient lift to stay airborne by overcoming the large viscous force while reducing wing mass and hence inertial power (Ellington 1980, Davidi & Weihs 2012, Santhanakrishnan et al. 2014, Jones et al. 2016, Cummins et al. 2018).

The flapping bristled wings of featherwing beetles (**Figure 4a**) display a pronounced figure-eight loop that comprises subperpendicular upstrokes and downstrokes followed by claps at stroke reversals above and below the body (**Figure 4b**), allowing these tiny insects to fly at speeds and accelerations of insects three times their size (Farisenkov et al. 2022). CFD simulations revealed a pair of strong VRs wrapping the paired bristled wings with the porous wing surface (**Figure 4c**), effectively minimizing airflow leakiness by remarkably reducing the overall inertial load (a 70–80% reduction in the wing area) compared with the membranous wing

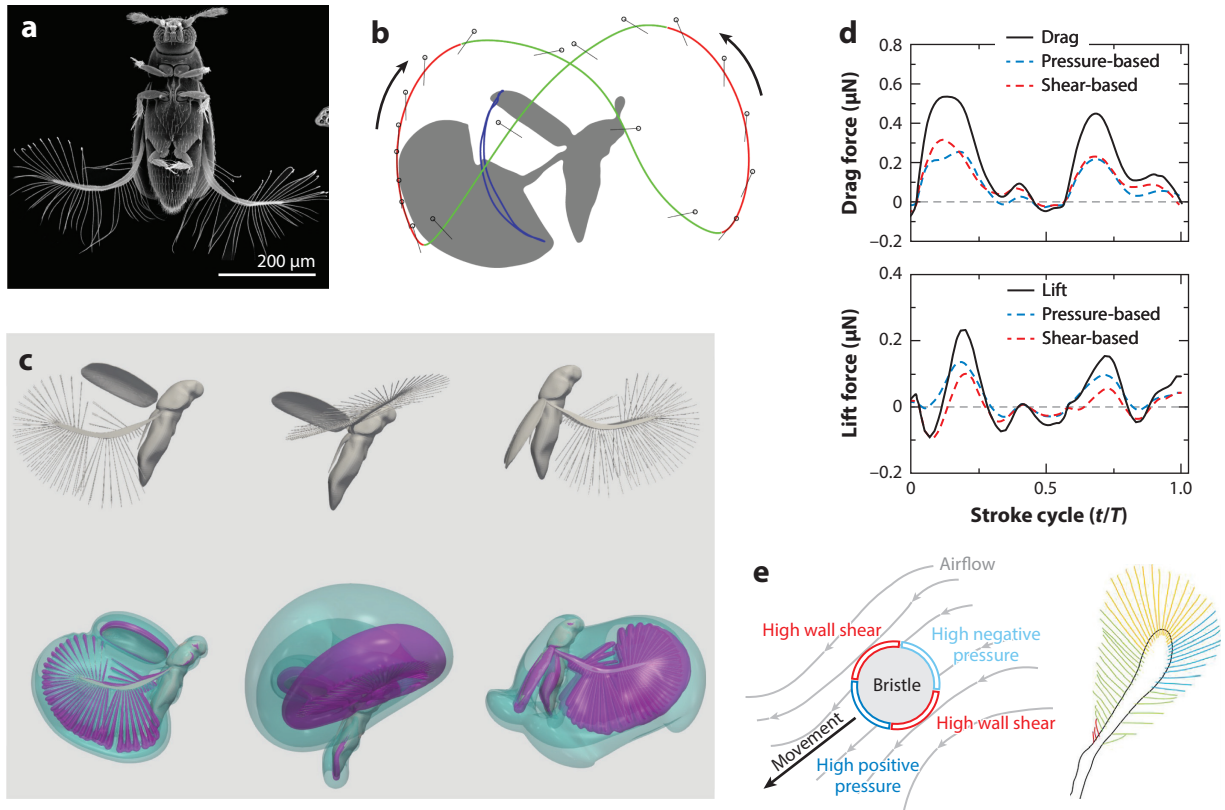


**Figure 4**

(a) Prominent wing morphology, (b) wing kinematics, and (c) flow structures for the tiny beetle *Paratiposa placentis*. Panels a–c adapted from Farisenkov et al. (2022). (d) Aerodynamic forces associated with (e) bristled wings of the wasp *Anagrus* Haliday. Panels d and e adapted from Jiang et al. (2022).

(Jiang et al. 2022) and utilizing a passive shear-shear-drag-enhancing mechanism to generate the requisite force (Figure 4d,e). On the basis of the decomposition of the vertical force exerted on the wing into both the pressure-based and the shear-stress-based drag and lift, researchers revealed that the vertical aerodynamic force benefits much more from the bristle-induced drag (Figure 4d) than from the lift in the bristled wings of wasps (Jiang et al. 2022) and featherwing beetles (Farisenkov et al. 2022). The pressure and shear-stress distributions around a circular cylinder model of the bristled wing (Figure 4e) present a pair of high wall-shear zones responsible for augmenting the production of friction-based drag. The pressure difference between the front and the rear parts contributes to the pressure-based drag, indicating an alternative low-*Re* aerodynamic mechanism distinct from the lift-based high-*Re* aerodynamic mechanism (Liu et al. 2016).

### 3.4. Wakes in Bird and Bat Flight

The flapping wings of birds generate complex wake vortices, footprints of the generated lift and thrust/drag (Maybury et al. 2001; Spedding et al. 2003a,b; Rosén et al. 2004, 2007; Hedenström et al. 2007; Hedenström & Spedding 2008; Johansson et al. 2008). The wake vortices of three gliding birds (a female barn owl, a male tawny owl, and a female northern goshawk) were measured by Usherwood et al. (2020), who further inferred that the body/tail section contributed the

lift as an effective flap deflected downward to support the bird's weight. This finding is consistent with other observations (Pennycuick et al. 1992, Maybury et al. 2001, KleinHeerenbrink & Hedenström 2017) and CFD simulations (Song et al. 2022). KleinHeerenbrink et al. (2017) measured TVs over a jackdaw, revealing multiple-core vortices generated by slotted wing tip feathers in both gliding and flapping flight and the resulting vortex-spreading as the mechanism of the induced drag reduction. Furthermore, the wake vortices of birds with highly dynamic and localized upwash and downwash could have the energetic benefit in V-formation flight (Portugal et al. 2014).

Complex wake vortices of bats differ from those of birds in some aspects (Hedenström et al. 2007, 2009). PIV-measured velocity fields of the wakes of Pallas's long-tongued bat and the southern long-nosed bat were presented by Hedenström et al. (2009). In general, the tube-like TVs trail the path of the wing tip and shed continuously throughout the wing stroke, forming incomplete ring-like vortices that travel downstream (Hubel et al. 2009). A pair of root vortices generated with the opposite spin to the same-side TV were observed mainly during the downstroke (Hedenström et al. 2007; Hubel et al. 2009, 2010; Muijres et al. 2011) and the upstroke (Muijres et al. 2011) in some species. The circulation can be calculated by integrating streamwise vorticity fields into the Trefftz plane (Hedenström et al. 2007; Johansson et al. 2008; Hubel et al. 2009, 2010).

## 4. AERODYNAMIC MODELS FOR FLAPPING FLIGHT

### 4.1. CFD Modeling

CFD modeling of unsteady aerodynamics for flapping flight needs an integrated methodology that incorporates the realistic body-wing morphology, the flapping-wing and body kinematics, the unsteady flapping-wing aerodynamics, and the quantitative evaluation of flapping energetics on the inertial and aerodynamic forces, torques, and powers (Liu 2009).

For the flows around a flapping wing in the low- and intermediate- $Re$  regime ( $Re = 10^0-10^6$ ) at low Mach number ( $Ma < 0.3$ ), the governing equations are the 3D unsteady incompressible Navier-Stokes equations and the continuity equation in a nondimensionalized vector form (Liu 2009), i.e.,

$$St \frac{\partial \mathbf{V}}{\partial t} + \mathbf{V} \cdot \nabla \mathbf{V} = -\nabla p + \frac{1}{Re} \nabla^2 \mathbf{V} \quad 1a.$$

and

$$\nabla \cdot \mathbf{V} = 0, \quad 1b.$$

where  $\mathbf{V} = (u, v, w)$  is the velocity vector,  $p$  is the pressure,  $t$  is the time, and  $\nabla$  is the gradient operator. The scaling parameters are  $Re$ ,  $St$  (Equation 1a), and the reduced frequency  $k$ , which are defined as  $Re = U_{\text{ref}} L_{\text{ref}} / \nu$ ,  $St = f L_{\text{ref}} / U_{\text{ref}}$ , and  $k = \pi f L_{\text{ref}} / U_{\text{ref}}$ , respectively, where  $U_{\text{ref}}$  denotes the reference velocity,  $L_{\text{ref}}$  is the reference length (the mean chord length  $c_m$ ),  $\nu$  is the kinematic viscosity, and  $f$  is the flapping frequency. For forward flight,  $U_{\text{ref}}$  is the forward flight speed. For hovering,  $U_{\text{ref}} = \omega R$  is the mean wing tip velocity, where  $R$  is the wing length,  $\omega = 2\Phi f$  is the mean angular velocity of the wing, and  $\Phi$  is the wing beat amplitude. Moreover, the advance ratio is defined by  $J = U_f / (2Af)$  and used to characterize the effects resulting from the reciprocating motion of a flapping wing, where  $U_f$  is the forward flight velocity and  $A$  is the flapping amplitude. The Rossby number,  $Ro$ , is used to characterize these rotational effects, which for hovering flight can also be interpreted more intuitively as the AR of a single wing with respect to the center of rotation. It ranges roughly from 1 to 10, with average values between 3 and 4 for hovering insects and vertebrates (Lentink & Dickinson 2009).

Here, we clarify the prominent issues with CFD modeling of unsteady aerodynamics in bioinspired flapping flight, including rigid-wing, flexible flapping-wing, and flexible wing-hinge models.

**4.1.1. Rigid-wing model.** The rigid-wing model is broadly used in CFD modeling to understand the essential vortex dynamics and aerodynamic forces of the flapping-wing motion prescribed based on either realistic or idealized wing kinematics models (Liu et al. 1998, Sun & Tang 2002, Liu 2009). It can capture the primary vortex-dominated unsteady aerodynamics in both hovering and forward flights over a broad range of insect species (Liu 2009, Xu et al. 2021, Xue et al. 2022). For instance, the flapping-wing aerodynamics in hawk moth hovering (Liu et al. 1998, Liu 2009) is prominently featured by near- and far-field vortices (**Figure 1b**). Whereas the wake topology presents considerable diversity in different species, the LEVs are uniformly present on their forewings in most cases (Thomas et al. 2004).

The vortex dynamics is responsible for force generation, as seen in the time course of the vertical force coefficient in **Figure 5a** in hawk moth hovering featuring twin peaks at downstrokes and upstrokes. The stable LEV is observed throughout the stroke cycle along with a compact and stable VR during the half-stroke (**Figure 1b**), which may stabilize the LEV and augment force production. The twin peaks result from the LEV breakdown at the late half-stroke (Liu 2009). As shown in **Figure 5b**, the energetics associated with flapping flight can be evaluated as the sum of the muscle-mass-specific inertial, aerodynamic, and total mechanical powers based on the transient aerodynamic forces and the wing velocities. The aerodynamic power  $P_{\text{aero}}$  required to overcome the drag reaches the maxima in the early phase of both downstrokes and upstrokes, and during the translation phase it displays a high value owing to LEV-dominated force production at high AoAs (**Figure 2b**). The stroke-averaged aerodynamic power is approximately  $90 \text{ W kg}^{-1}$ , which is consistent with the measurements (Liu 2009). The inertial power  $P_{\text{iner}}$  for flapping the wing increases (or decreases) as the wing accelerates (or decelerates). Here, it is assumed that wing deceleration accrues with no cost and that there is no elastic storage, which results in a mean inertial power of  $65 \text{ W kg}^{-1}$ . The total mechanical power  $P_{\text{total}}$  is the sum of the aerodynamic and inertial powers, producing the twin peaks in the early downstrokes and upstrokes (Liu 2009).

The LEVs are confirmed as the convergent mechanism responsible for creating most of the aerodynamic force in hawk moth forward flight, and the body vortices induced by wing-body

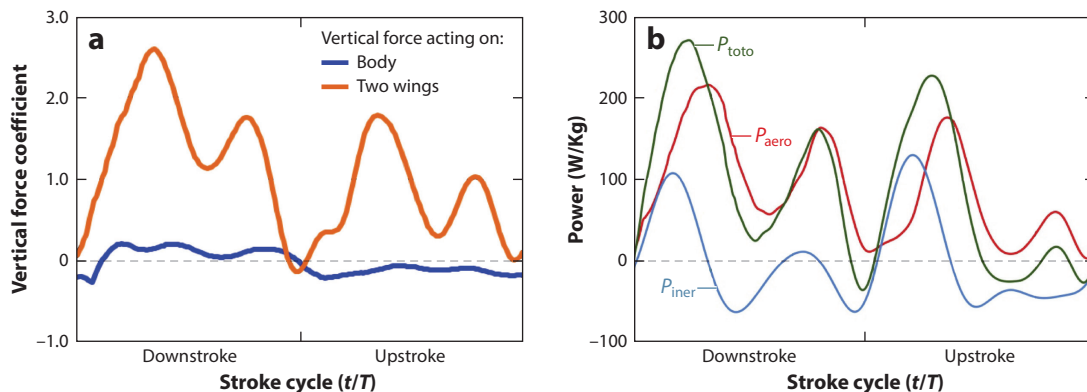


**Figure 5**

Time courses of (a) the vertical force coefficient ( $C_v$ ) and (b) muscle-mass-specific inertial ( $P_{\text{iner}}$ ), aerodynamic ( $P_{\text{aero}}$ ), and total mechanical ( $P_{\text{total}}$ ) powers in a rigid-wing model of hawk moth hovering. Figure adapted from Liu (2009).

interactions (**Figure 1c**) can augment the vertical force at all flight velocities, producing a 10% increase in fast flights (Xue et al. 2022). The time-averaged body-mass-specific mechanical power produces a J-shaped curve, reducing the power cost in intermediate- and high-velocity flights and saving energy through the wing-body interaction. High-AR wings increase wing- and body-based vertical forces. Furthermore, realistic wing-to-body mass ratios lead to a low power cost, and a slightly reduced frequency optimizes aerodynamic performance.

**4.1.2. Flexible-wing model.** The wings of natural flyers are composed of flexible membranes or feathers, changing their 3D shapes passively and dynamically in response to the aerodynamic and inertial forces in flapping flight. The fluid-structure interaction (FSI) between flexible wings and the surrounding fluid that determines wing deformation and aerodynamic performance is modeled by coupling the structural dynamics and aerodynamics of the flexible flapping wing (Shyy et al. 2010; Nakata & Liu 2012a,b). Measurements and FSI simulations indicate that the inertial force on flapping wings likely serves as the major determinant of flapping-wing deformation but that the aeroelastic contribution could enhance the aerodynamic performance of flapping wings owing to the dynamic response of a flexible flapping wing (Combes & Daniel 2003, Sims et al. 2010, Zheng et al. 2012).

Compared with the aerodynamics of the rigid-wing model, flexible-wing aerodynamics shows a significant difference in terms of vortex dynamics and aerodynamic performance. For a hovering hawk moth (Nakata & Liu 2012a,b), the dynamic wing deformation and velocity owing to wing flexibility can enhance the LEV and hence the production of aerodynamic force (**Figure 6b-d**). Dynamic wing bending (**Figure 6a**) delays the breakdown of the LEV near the wing tip (**Figure 6c**), resulting in noticeably lower pressure distributions (**Figure 6d**) while augmenting the production of stroke-averaged vertical force by 20%. A combination of dynamic wing bending and twist can increase the mechanical efficiency of hovering by 13%. For a locust in forward flight, wing deformation enhances efficiency by aligning the leading edge with the flow to avoid flow separation (Young et al. 2009). For a beetle, dynamic twist can increase the lift while camber variation increases the thrust but decreases the aerodynamic power (Le et al. 2013). Much larger increases in lift and power savings were observed in a computational butterfly model with flexible wings, and twist deformation was identified to have the strongest effect on aerodynamic performance (Zheng et al. 2012).

The resonance of flexible wings to the wingbeat frequency may play a crucial role in flapping flight, since flapping wings may be able to store and release the energy for flapping motion (Dickinson & Lighton 1995). Measurements in various insects show a wingbeat frequency lower than the natural frequency (Sunada et al. 1998, Chen et al. 2008, Ha et al. 2013), suggesting that insects may use the enhanced aerodynamic performance by manipulating the phase lag between wing rotation and translation rather than matching the wingbeat frequency to the natural frequency (Vanella et al. 2009, Yin & Luo 2010, Ramananarivo et al. 2011, Dai et al. 2012, Sridhar & Kang 2015). Researchers have proposed some scaling laws for force generation and efficiency by using simplified computational and physical models of a flapping wing (Kang et al. 2011, Kodali & Kang 2016), suggesting that maximum force may be achieved when flapping near the structural resonance (Kang & Shyy 2014) but that efficiency depends on the nonlinear FSI effects (Ramananarivo et al. 2011, Bergou et al. 2010).

**4.1.3. Flexible wing-hinge model.** Flying insects can perform robust flapping-wing dynamics under various environments while minimizing the energetic cost by using elastic wing hinges (Dickinson & Lighton 1995). Under the interplay between the inertial, aerodynamic, and elastic restoring forces, the flapping-wing motion is constrained by the flexible wing hinges, which alters

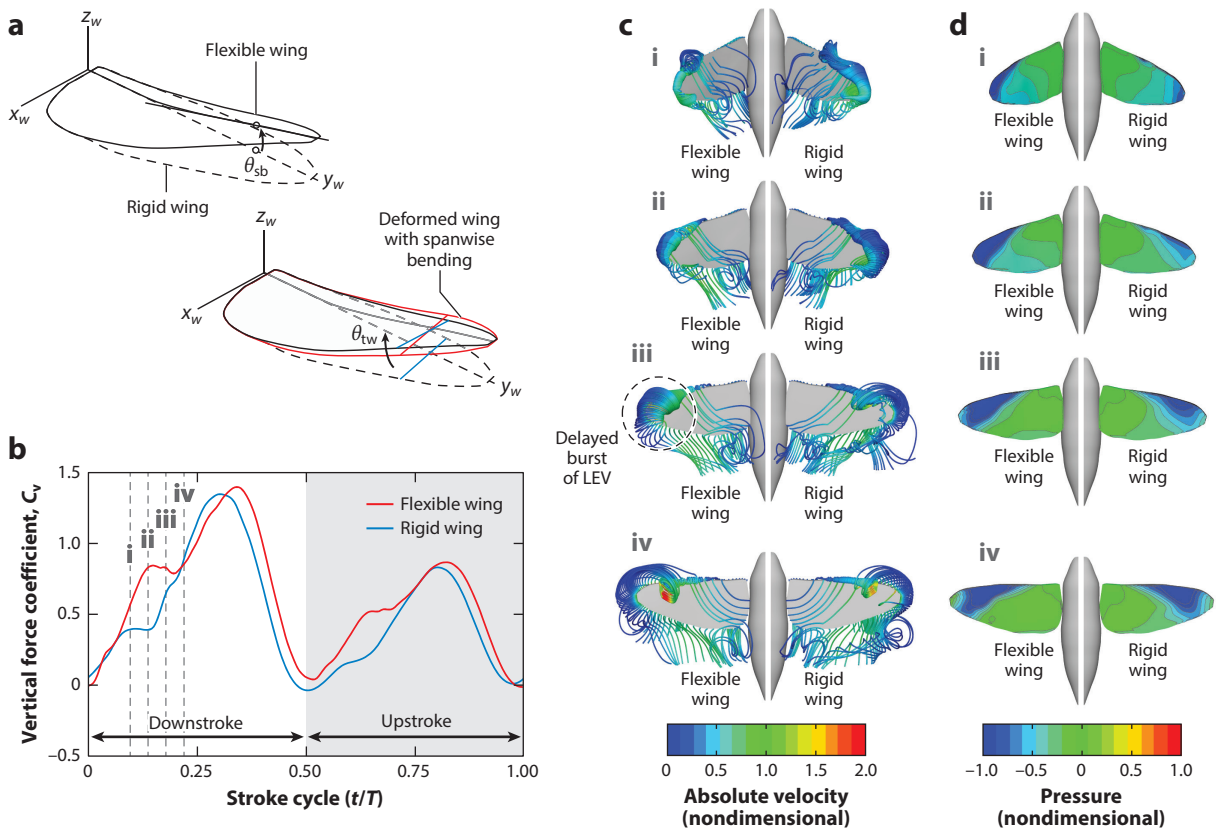


**Figure 6**

(a) Wing deformations (twist and bending), (b) time course of the vertical force coefficient, (c) instantaneous streamlines, and (d) pressure contours on the upper surface of flexible and rigid wings (at four instances: i, ii, iii, and iv) in hawk moth hovering, where  $\theta_{sb}$  is the spanwise bending angle and  $\theta_{tw}$  is the twist angle. Abbreviation: LEV, leading-edge vortex. Figure adapted from Nakata & Liu (2012a,b).

the wing kinematics and hence the flapping aerodynamics in a passive way (Bergou et al. 2010). The passive pitching associated with flapping-wing kinematics has been investigated experimentally (Ishihara et al. 2014) and computationally by a coupled FSI method between the flexible wing-hinge and the surrounding fluid (Kolomenskiy et al. 2019), demonstrating that passive feathering can be achieved based on a torsional spring model (Figure 7a) and that it can generate sufficient lift to support the weight of insects.

The interplay between the passive rotation owing to wing-hinge flexibility, wing inertia, and aerodynamic force determines the robustness and efficiency of flapping dynamics, aerodynamic performance, and flight stabilization (Liu 2020). Cai et al. (2022) recently proposed an FSI model coupled with unsteady flapping aerodynamics and three-torsional-spring-based elastic wing-hinge dynamics to determine passive and active mechanisms (PAMs) in bumble bee hovering (Liu 2020). The results show that a strategy of active-controlled stroke, passive-controlled wing pitch, and deviation enables optimal elastic storage (Figure 7b,c). The robust flapping-wing dynamics characterized by dynamics-based passive elevation rotation and aerodynamics-based passive feathering rotation can produce the aerodynamic forces while achieving the high power efficiency over a

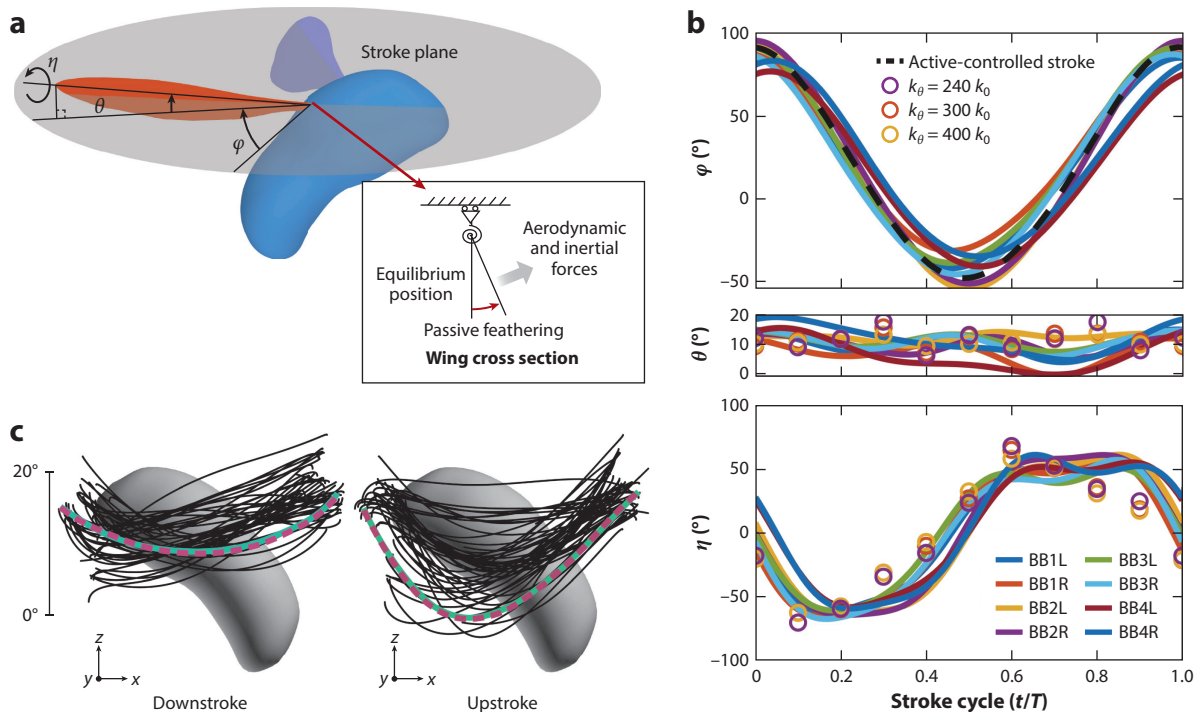


**Figure 7**

Flapping-wing dynamics with a flexible wing hinge. (a) Definition of wing kinematics, where  $\phi$  is the positional angle,  $\theta$  is the elevation angle, and  $\eta$  is the feathering angle, and the stroke plane of a hovering bumble bee. (b) Time-varying angles ( $\phi$ ,  $\theta$ ,  $\eta$ ) of four individuals measured (*solid lines*) and results based on an elastic wing-hinge model (*circles*) at various elevation-spring stiffnesses. (c) Wing deviations (elevation angle). Black lines indicate measurements of the wing kinematics of the left and right wings of four individual bumble bees (BB1L–BB4L, BB1R–BB4R), light green lines indicate measurements of the right wing kinematics of a bumble bee (BB1R), and dashed magenta lines indicate the measurements of the right wing fitted kinematics of a bumble bee (BB1R). Figure adapted from Cai et al. (2022).

broad range of wing-hinge stiffnesses. A force–impulse model further confirms the capability of external perturbation robustness under the PAM-based strategy (Cai et al. 2022).

## 4.2. Quasi-Steady Model

The quasi-steady model is a fast and efficient analytical method to estimate the time-dependent aerodynamic forces of a flapping wing under the quasi-steady assumption given the motion of the wing (Sane & Dickinson 2002). As shown in **Figure 8**, the quasi-steady model normally includes the translational terms, the added-mass term, the rotational terms (van Veen et al. 2019), and the blade element term (Glauert 1983). The wing is divided into a series of thin elements, and each element has its velocity and acceleration, on which the quasi-steady model is constructed to calculate the aerodynamic force, torque, and power.

The quasi-steady model proposed by Cai et al. (2021) was employed for a range of insect flight velocities (forward/backward velocity, lateral velocity, and vertical velocity). The aerodynamic force  $F_{\text{aero}}$  generated by the flapping wing can be decomposed into five quasi-steady forces based on the blade element method (**Figure 8**): translational circulation force ( $F_{\text{tc}}$ ), rotational circulation force ( $F_{\text{rc}}$ ), translational drag ( $F_{\text{td}}$ ), rotational drag ( $F_{\text{rd}}$ ), and force due to added mass ( $F_{\text{am}}$ ).

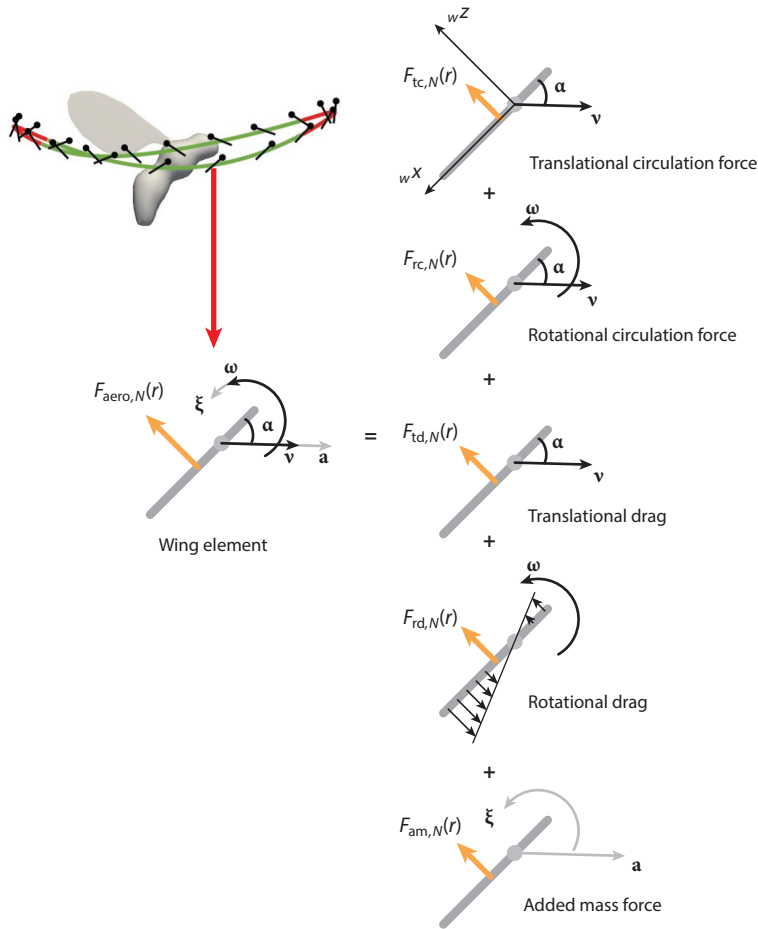


**Figure 8**

Illustration of the quasi-steady model of a flapping wing. (*Left*) Total aerodynamic force ( $F_{\text{aero}}$ ) and (*right*) five decomposed quasi-steady force terms, translational circulation force ( $F_{\text{tc}}$ ), rotational circulation force ( $F_{\text{rc}}$ ), translational drag ( $F_{\text{td}}$ ), rotational drag ( $F_{\text{rd}}$ ), and force due to added mass ( $F_{\text{am}}$ ), on a wing element. Figure adapted from Cai et al. (2021).

For insect flight, the aerodynamic force acting on the flapping wings is dominated by the pressure force acting on the wing surface, and thus it can be reasonably assumed to be normal to the wing surface (Sane & Dickinson 2002, Nakata et al. 2015, Wang et al. 2016). Thus, the normal component of the aerodynamic force can be calculated as the sum of the five force terms, i.e.,

$$F_{\text{aero},N} = F_{\text{tc},N} + F_{\text{rc},N} + F_{\text{td},N} + F_{\text{rd},N} + F_{\text{am},N}, \quad 2.$$

where the five force terms can be expressed as functions of the local chordwise length, the local velocity component, the force coefficients of these terms in Equation 2, and the feathering angle (the local AoA). The total aerodynamic force of the wing can be obtained by integrating the force on each wing element over the wing.

To close this quasi-steady model, researchers have theoretically (Sedov 1965), experimentally (Dickinson et al. 1999, Sane & Dickinson 2002, Whitney & Wood 2010), and computationally (Pesavento & Wang 2004, Nakata et al. 2015, Bluman & Kang 2017) determined the force

coefficients. These coefficients were determined by fitting the instantaneous aerodynamic forces obtained from a high-fidelity computational model (Liu 2009) with the least-squares method for hovering flight (Nakata et al. 2015) and for forward flight (Cai et al. 2021). It has been verified that increasing the size of input CFD databases with different wing kinematics can improve the accuracy of the quasi-steady model. Furthermore, to resolve the trade-off between the computational complexity of the unsteady aerodynamic model and its accuracy, Cai et al. (2021) proposed the so-called CFD-informed quasi-steady modeling methodology to determine the quasi-steady model coefficients based on CFD simulations, in which the nonlinear unsteady aerodynamic effects dominated by vortex flows were incorporated.

### 4.3. Vortex Lift Model

Vortex lift models are useful for estimating the lift contributions by dominant vortex structures generated by natural flyers (LEVs and wake vortices) and for evaluating the effects of relevant parameters such as dynamic wingspan and wing sweep in flapping flight.

**4.3.1. Two-term lift decomposition.** To calculate the lift of a flapping wing, Wang et al. (2013) gave the two-term lift decomposition,

$$L \approx L_{\text{vor}} + L_a = \rho \mathbf{k} \cdot \int_{V_f} \mathbf{u} \times \boldsymbol{\omega} dV - \rho \mathbf{k} \cdot \frac{d}{dt} \int_{V_f} \mathbf{u} dV, \quad 3.$$

where  $\mathbf{u}$  is the velocity,  $\boldsymbol{\omega}$  is the vorticity,  $\rho$  is the fluid density,  $\mathbf{k}$  is the unit vector normal to the freestream velocity, and  $V_f$  denotes the control volume of fluid. The vortex lift  $L_{\text{vor}}$  is the volume integral of the Lamb vector  $\mathbf{l} = \mathbf{u} \times \boldsymbol{\omega}$ , which is the main contribution of the time-averaged lift  $\langle L \rangle_T \approx \langle L_{\text{vor}} \rangle_T$  in both steady flight and flapping flight, where  $\langle \bullet \rangle_T$  is the time-averaging operator over a flapping period.  $L_a$  is the lift associated with the acceleration of fluid (the added-mass lift in an inviscid irrotational flow). This decomposition is sufficiently accurate for complex, unsteady viscous flows generated by a flapping wing enclosed in a sufficiently large but finite rectangular outer control surface (approximately 6 chord lengths from a wing). A similar decomposition can be obtained for the drag and power if the finite control surface is taken as a special wedge domain or as particular vortex surfaces (Li & Lu 2012, Tong et al. 2021). This decomposition can give the nonlinear vortex lift in complex unsteady separated flows that cannot be accurately modeled by classical potential-flow-based lift models.

**4.3.2. Vortex lift enhanced by dynamic wing morphing.** The vortex lift model has been used to analyze lift enhanced by dynamic wing morphing. The wingspan and wing planform of a flapping flying bird (or bat) are actively changed, which is generally considered dynamic wing morphing. To gain a clear understanding of the aerodynamics of dynamic wing morphing, Wang et al. (2014) studied a flapping rectangular flat-plate wing with a dynamically changing wingspan, simulating a morphing flapping wing of a bird (or bat). They found that the LEVs on the upper surface are significantly intensified by the spanwise vortex stretching associated with a dynamically changing wingspan, contributing to the elevated vortex lift in a range of span ratios.

Further, Wang et al. (2014, 2015a,b) investigated vortex lift in models of flapping bat wings with different span ratios. The vertical component of the Lamb vector ( $l_z$ ) associated with the LEVs is significantly intensified by a dynamically changing wingspan (**Figure 9a-d**), contributing to the enhanced vortex lift (**Figure 9e,f**), whereas the temporal variation of the lift associated with the fluid acceleration remains roughly unchanged. Therefore, the interaction between dynamic wing morphing and LEVs enhances lift for a flying bat.

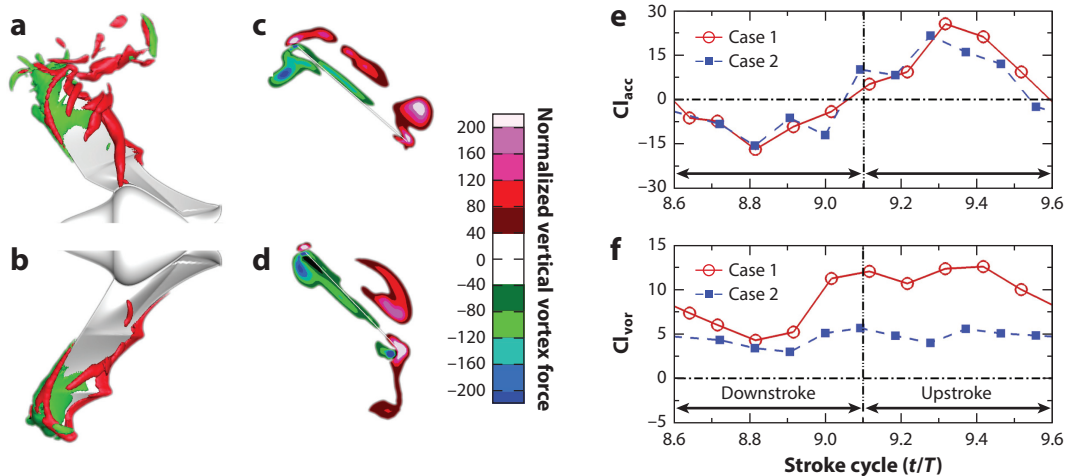


**Figure 9**

The distributions of the vertical component of the Lamb vector ( $L_z$ ) around the bat wings at  $t/T = 0.2$  after the start of the upstroke, where  $T$  is the flapping period. The top views of the isosurface of  $L_z$  in (a) the dynamically changing wingspan case (on the right wing, Case 1) and (b) the fixed wingspan case (on the left wing, Case 2). The distributions of  $L_z$  in the slices at 60% of the semi-wingspan from the body in (c) Case 1 and (d) Case 2. (e) The lift coefficients associated with the fluid acceleration term ( $Cl_{acc}$ ) and (f) the vortex lift ( $Cl_{vor}$ ) in Case 1 and Case 2. Figure adapted from Wang et al. (2015a).

**4.3.3. Vortex lift enhanced by wing sweep.** A bird or bat usually sweeps the hand-wing during flapping flight (wing sweep morphing). Wang et al. (2022) studied an optimization problem in a model of a two-joint flapping bird wing with sweep morphing (Liu et al. 2006) to maximize the time-averaged lift generated by the LEVs in a parametric space of the relevant geometrical and kinematical parameters, particularly the hand-wing sweep morphing. The distributions of the Lamb vector component ( $L_z$ ) normal to the incoming flow indicate the stronger LEVs of the arm-wing and hand-wing attached more tightly to the upper surface due to hand-wing sweep morphing. The enhancement of the vortex lift of the morphing hand-wing dominates the optimal performance of the wing.

**4.3.4. Vortex lift and wake.** Simplified quasi-steady wake models (such as the Kutta–Joukowski theorem) often underpredict the time-averaged lift, especially in slow-flying cases (Hubel et al. 2009, Gutierrez et al. 2017). To incorporate the evolutionary effects of complex wake vortices on both their strength and spanwise scale of a flapping wing (Equation 3), Wang et al. (2019) gave the wake-sectional Kutta–Joukowski (WS-KJ) model. When the wake structures in the Trefftz plane at a streamwise location are symmetrical, the time-averaged vortex lift is written as

$$\langle L_{vor} \rangle_T = \rho U \langle b_{vor} \rangle_T \langle \Gamma \rangle_T, \quad 4.$$

where  $\langle \Gamma \rangle_T$  is the time-averaged circulation that is the integral of the streamwise vorticity on the right-hand side of the Trefftz plane,  $U$  is the incoming flow velocity, and  $\langle b_{vor} \rangle_T$  is the vorticity-weighted width of the wake. The accuracy of the WS-KJ model has been validated by Wang et al. (2019) on the basis of the numerical simulations of low- $Re$  flows over flapping-wing models with different wing geometry and kinematics. Another approach is the use of data-driven models based on the convolutional neural network that achieve better accuracy than do conventional theoretical models for the estimation of aerodynamic forces from wake velocity data (Tong et al. 2022).

## SUMMARY POINTS

1. While insects, bats, and birds are diverse in their wing morphology and flapping kinematics, they share the essential physics of vortex-dominated unsteady flapping aerodynamics in the low- and intermediate-Reynolds-number ( $Re$ ) regime of  $10^0$  to  $10^6$ .
2. The leading-edge vortex (LEV) is a convergent and robust mechanism for aerodynamic force generation in the translation stroke of flapping wings at all  $Re$  (sizes) of insects and vertebrates, which can be intensified by wing flexibility in insects and wing morphing (including dynamically changing wingspan and hand-wing sweep) in birds and bats. The instability of the LEVs is caused by von Kármán–vortex-type shedding instability, Kelvin–Helmholtz instability, vortex breakdown, and Coriolis force.
3. In insect flight, lift-generating vortices are also observed during wing rotation of the wingbeat stroke, which are associated with the Framer effect, clap-and-fling mechanism, and wing-wake interaction.
4. Very small insects utilize vortices generated by their bristled wings to achieve a novel drag-based flight performance by overcoming the large viscous forces while reducing wing mass and inertial power in very-low- $Re$  ( $<40$ ) flow regimes.
5. In bird and bat flight, complex wake vortices due to interactions between the streamwise tube-like wing tip vortices and the spanwise shedding LEVs in the wing strokes provide the footprints of the generation of lift and thrust/drag. Therefore, the time-averaged lift of a flapping wing can be estimated from wake velocity data based on vortex lift models.
6. Computational fluid dynamics (CFD) modeling provides an integrated methodology to quantify the vortices and forces in association with rigid and flexible wings and flexible wing hinge in terms of wing–body, fluid–structure, and aeroelastic interactions. The quasi-steady model can provide a fast and efficient analytical method to estimate the flapping-wing aerodynamic forces, with the force coefficients determined by CFD and CFD-informed modeling and measurements. Vortex lift models for bird and bat flight can estimate the lift force by combining the time-averaged vortex lift and the fluid-acceleration-related temporal variation of the lift.

## FUTURE ISSUES

1. Vortices and forces in biological flight are actively produced by wing motions while passively enhanced owing to the flexibility of the wing and wing hinge by adjusting wing shape and kinematics and to adaptive muscle stiffness. Such a passive and active mechanism strategy remains an open question; that is, How do the flexible structures work interactively and complementarily to produce robust aerodynamic forces?
2. Flying insects, bats, and birds can achieve efficient and robust flight performance in turbulent flows by positive and passive adjustments on wingbeat kinematics and body altitudes corresponding to the intensity, scale, and regularity of turbulence. It is highly challenging to measure, simulate, and model flow transition and near-wall turbulence on moving surfaces in biological flight. Furthermore, turbulence rejection, which remains unclear and unexplored, is an extreme challenge of unsteady aerodynamics in biological flight.

3. Morphologies and structures of the vein–membrane and bristled wings of insects, the membranous wings of bats, and the feathered wings of birds significantly affect vortex dynamics and aerodynamic forces. A good understanding of these effects requires an integration of multiscale aerodynamics consisting of the wing-motion-induced macrofluid (large-scale) mechanics and the vein–membrane–feather-induced microfluid (small-scale) mechanics.
4. Fluid–structure interaction and multiscaled modeling in association with biological flight present great challenges owing to diverse, flexible, and multiscaled structures and complex wing motions. For bird and bat flight at intermediate  $Re$ , modeling flow transition and near-wall turbulence on moving surfaces is particularly arduous. In experiments, measuring complex 3D unsteady flows, aerodynamic forces, and wing motion of natural flyers simultaneously is difficult, although some highly simplified mechanical models have been used to mimic certain physical aspects of flapping flight of natural flyers.

## DISCLOSURE STATEMENT

The authors are not aware of any biases that might be perceived as affecting the objectivity of this review.

## ACKNOWLEDGMENTS

S.W. is supported by the National Natural Science Foundation of China Basic Science Center Program for Multiscale Problems in Nonlinear Mechanics (grant 11988102). T.L. is supported by the Presidential Innovation Professorship and the John O. Hallquist Endowed Professorship at Western Michigan University. H.L. acknowledges research funding from the Japan Society for the Promotion of Science (JSPS) KAKENHI grants 21360078, 24120007, and 19H02060. He thanks all the members of the bioflight group at Chiba University for their valuable contributions.

## LITERATURE CITED

- Amador LI, Almeida FC, Giannini NP. 2020. Evolution of traditional aerodynamic variables in bats (Mammalia: Chiroptera) within a comprehensive phylogenetic framework. *J. Mamm. Evol.* 27:549–61
- Beatus T, Cohen I. 2015. Wing-pitch modulation in maneuvering fruit flies is explained by an interplay between aerodynamics and a torsional spring. *Phys. Rev. E* 92:022712
- Bender M, Tian L, Fan X, Kurdila A, Mueller R. 2019. Spatially recursive estimation and Gaussian process dynamic models of bat flapping flight. *Nonlinear Dyn.* 95:217–37
- Bergou AJ, Ristroph L, Guckenheimer J, Cohen I, Wang ZJ. 2010. Fruit flies modulate passive wing pitching to generate in-flight turns. *Phys. Rev. Lett.* 104:148101
- Birch JM, Dickinson MH. 2003. The influence of wing–wake interactions on the production of aerodynamic forces in flapping flight. *J. Exp. Biol.* 206:2257–72
- Bluman J, Kang C-K. 2017. Wing-wake interaction destabilizes hover equilibrium of a flapping insect-scale wing. *Bioinspiration Biomim.* 12:046004
- Bomphrey RJ, Lawson NJ, Harding NJ, Taylor GK, Thomas AR. 2005. The aerodynamics of *Manduca sexta*: digital particle image velocimetry analysis of the leading-edge vortex. *J. Exp. Biol.* 208:1079–94
- Bomphrey RJ, Nakata T, Phillips N, Walker SN. 2018. Smart wing rotation and trailing-edge vortices enable high frequency mosquito flight. *Nature* 44:92–95
- Brodsky AK. 1991. Vortex formation in the tethered flight of the peacock butterfly *Inachis io* L. (Lepidoptera, Nymphalidae) and some aspects of insect flight evolution. *J. Exp. Biol.* 161:77–95

- Cai X, Kolomenskiy D, Nakata T, Liu H. 2021. A CFD data-driven aerodynamic model for fast and precise prediction of flapping aerodynamics in various flight velocities. *J. Fluid Mech.* 915:A114
- Cai X, Xue YJ, Kolomenskiy D, Xu R, Liu H. 2022. Elastic storage enables robustness of flapping wing dynamics. *Bioinspiration Biomim.* 17:045003
- Carr ZR, DeVoria AC, Ringuette MJ. 2015. Aspect-ratio effects on rotating wings: circulation and forces. *J. Fluid Mech.* 767:497–525
- Carruthers AC, Walker SM, Thomas ALR, Taylor GK. 2010. Aerodynamics of aerofoil sections measured on a free-flying bird. *Proc. Inst. Mech. Eng. G* 224:855
- Chen D, Kolomenskiy D, Liu H. 2017a. Closed-form solution for the edge vortex of a revolving plate. *J. Fluid Mech.* 821:200–18
- Chen D, Kolomenskiy D, Nakata T, Liu H. 2017b. Wing morphology matches the formation of leading-edge vortices in a revolving insect wing. *Bioinspiration Biomim.* 13:016009
- Chen D, Lentink D. 2016. Flapping wing aerodynamics: from insects to vertebrates. *J. Exp. Biol.* 219:920–32
- Chen JS, Chen JY, Chou YF. 2008. On the natural frequencies and mode shapes of dragonfly wings. *J. Sound Vib.* 313:643–54
- Combes SA, Daniel TL. 2003. Flexural stiffness in insect wings. I. Scaling and the influence of wing venation. *J. Exp. Biol.* 206:2979–87
- Cummins C, Seale M, Macente A, Certini D, Mastropaolo E, et al. 2018. A separated vortex ring underlies the flight of the dandelion. *Nature* 562:414–18
- Dai H, Luo H, Doyle JF. 2012. Dynamic pitching of an elastic rectangular wing in hovering motion. *J. Fluid Mech.* 693:473–99
- Davidi G, Weihs D. 2012. Flow around a comb wing in low-Reynolds-number flow. *ALAA J.* 50:249–53
- Dickinson MH, Lehmann FO, Sane SP. 1999. Wing rotation and the aerodynamic basis of insect flight. *Science* 284:1954–60
- Dickinson MH, Lighton JRB. 1995. Muscle efficiency and elastic storage in the flight motor of *Drosophila*. *Science* 268:87–90
- Eldredge JD, Jones AR. 2019. Leading-edge vortices: mechanics and modeling. *Annu. Rev. Fluid Mech.* 51:75–104
- Ellington CP. 1980. Wing mechanics and take-off preparation of thrips (Thysanoptera). *J. Exp. Biol.* 85:129–36
- Ellington CP, van den Berg C, Willmott AP, Thomas ALR. 1996. Leading-edge vortices in insect flight. *Nature* 384:626–30
- Engels T, Kolomenskiy D, Schneider K, Lehmann FO, Sesterhenn J. 2016. Bumblebee flight in heavy turbulence. *Phys. Rev. Lett.* 116:028103
- Farisenkov SE, Kolomenskiy D, Petrov PN, Engels T, Lapina NA, et al. 2022. Novel flight style and light wings boost flight performance of tiny beetles. *Nature* 602:96–100
- Farisenkov SE, Lapina NA, Petrov PN, Polilov AA. 2020. Extraordinary flight performance of the smallest beetles. *PNAS* 117:24643–45
- Garmann DJ, Visbal MR. 2014. Dynamics of revolving wings for various aspect ratios. *J. Fluid Mech.* 748:932–56
- Glauert H. 1983. *The Elements of Aerofoil and Airscrew Theory*. Cambridge, UK: Cambridge Univ. Press
- Gutierrez E, Quinn DB, Chin DD, Lentink D. 2017. Lift calculations based on accepted wake models for animal flight are inconsistent and sensitive to vortex dynamics. *Bioinspiration Biomim.* 12:016004
- Ha NS, Truong QT, Goo NS, Park HC. 2013. Relationship between wingbeat frequency and resonant frequency of the wing in insects. *Bioinspiration Biomim.* 84:046008
- Harbig RR, Sheridan J, Thompson MC. 2013. Reynolds number and aspect ratio effects on the leading-edge vortex for rotating insect wing planforms. *J. Fluid Mech.* 717:166–92
- Harbig RR, Sheridan J, Thompson MC. 2014. The role of advance ratio and aspect ratio in determining leading-edge vortex stability for flapping flight. *J. Fluid Mech.* 751:71–105
- Hedenström A, Johansson LC. 2015. Bat flight: aerodynamics, kinematics and flight morphology. *J. Exp. Biol.* 218:653–63
- Hedenström A, Johansson LC, Wolf IM, Busse R, Winter Y, Spedding GR. 2007. Bat flight generates complex aerodynamic tracks. *Science* 316:894–97

- Hedenström A, Muijres FT, Busse R, Johansson LC, Winter Y, Spedding GR. 2009. High-speed stereo DPIV measurement of wakes of two bat species flying freely in a wind tunnel. *Exp. Fluids* 46:923–32
- Hedenström A, Spedding G. 2008. Beyond robins: aerodynamic analyses of animal flight. *J. R. Soc. Interface* 5:595–601
- Hubel TY, Hristov NI, Swartz SM, Breuer KS. 2009. Time-resolved wake structure and kinematics of bat flight. *Exp. Fluids* 46:933–43
- Hubel TY, Riskin DK, Swartz SM, Breuer KS. 2010. Wake structure and wing kinematics: the flight of the lesser dog-faced fruit bat, *Cynopterus brachyotis*. *J. Exp. Biol.* 213:3427–40
- Ishihara D, Horie T, Niho T. 2014. An experimental and three-dimensional computational study on the aerodynamic contribution to the passive pitching motion of flapping wings in hovering flies. *Bioinspiration Biomim.* 9:046009
- Jardin T, David L. 2015. Coriolis effects enhance lift on revolving wings. *Phys. Rev. E* 91:031001
- Jaworski JW, Peake N. 2020. Aeroacoustics of silent owl flight. *Annu. Rev. Fluid Mech.* 52:395–420
- Jiang Y, Zhao P, Cai X, Rong J, Dong Z, et al. 2022. Bristled-wing design of materials, microstructures and aerodynamics enables flapping flight in tiny wasps. *iScience* 25:103692
- Johansson LC, Wolf M, von Busse R, Winter Y, Spedding GR, Hedenström A. 2008. The near and far wake of Pallas' long tongued bat (*Glossophaga soricina*). *J. Exp. Biol.* 211:2909–18
- Jones SK, Miller LA, Yun YJJ, Hedrick TL, Griffith BE, Miller LA. 2016. Bristles reduce the force required to 'fling' wings apart in the smallest insects. *J. Exp. Biol.* 219:3759–72
- Kang C-K, Aono H, Cesnik CES, Shyy W. 2011. Effects of flexibility on the aerodynamic performance of flapping wings. *J. Fluid Mech.* 689:32–74
- Kang C-K, Shyy W. 2014. Analytical model for instantaneous lift and shape deformation of an insect-scale flapping wing in hover. *J. R. Soc. Interface* 11:20140933
- Kim D, Gharib M. 2010. Experimental study of three-dimensional vortex structures in translating and rotating plates. *Exp. Fluids* 49:329–39
- KleinHeerenbrink M, Hedenström A. 2017. Wake analysis of drag components in gliding flight of a jackdaw (*Corvus monedula*) during moult. *Interface Focus* 7:20160081
- KleinHeerenbrink M, Johansson LC, Hedenström A. 2017. Multi-cored vortices support function of slotted wing tips of birds in gliding and flapping flight. *J. R. Soc. Interface* 14:20170099
- Kodali D, Kang C-K. 2016. An analytical model and scaling of chordwise flexible flapping wings in forward flight. *Bioinspiration Biomim.* 12:016006
- Koekkoek G, Muijres FT, Johansson LC, Stuijver M, Oudheusden BW, Hedenström A. 2012. Stroke plane angle controls leading edge vortex in a bat-inspired flapper. *C. R. Mec.* 340:95–106
- Kolomenskiy D, Elimelech Y, Schneider K. 2014. Leading-edge vortex shedding from rotating wings. *Fluid Dyn. Res.* 46:031421
- Kolomenskiy D, Ravi S, Xu R, Ueyama K, Jakobi T, et al. 2019. The dynamics of passive feathering rotation in hovering flight of bumblebees. *J. Fluid Struct.* 91:102628
- Kruyt JW, Heijst GF, Altshuler DL, Lentink D. 2015. Power reduction and the radial limit of stall delay in revolving wings of different aspect ratio. *J. R. Soc. Interface* 12:20150051
- Le TQ, Truong TV, Park SH, Truong TQ, Ko JH, et al. 2013. Improvement of the aerodynamic performance by wing flexibility and elytra-hind wing interaction of a beetle during forward flight. *J. R. Soc. Interface* 10:20130312
- Lehmann FO, Pick S. 2007. The aerodynamic benefit of wing-wing interaction depends on stroke trajectory in flapping insect wings. *J. Exp. Biol.* 210:1362–77
- Lehmann FO, Sane SP, Dickinson MH. 2005. The aerodynamic effects of wing-wing interaction in flapping insect wings. *J. Exp. Biol.* 208:3075–92
- Lentink D, Dickinson MH. 2009. Biofluiddynamic scaling of flapping, spinning and translating fins and wings. *J. Exp. Biol.* 212:2691–704
- Lentink D, Müller UK, Stamhuis EJ, de Kat R, van Gestel W, et al. 2007. How swifts control their glide performance with morphing wings. *Nature* 446:1082–85
- Li GJ, Lu XY. 2012. Force and power of flapping plates in a fluid. *J. Fluid Mech.* 712:598–613
- Lighthill J. 1975. On the Weis-Fogh mechanism of lift generation. In *Mathematical Biofluidynamics*, pp. 179–95. Philadelphia: SIAM

- Limacher E, Morton C, Wood D. 2016. On the trajectory of leading edge vortices under the influence of Coriolis acceleration. *J. Fluid Mech.* 800:R1
- Linehan T, Mohseni K. 2020. Scaling trends of bird's alular feathers in connection to leading-edge vortex flow over hand-wing. *Sci. Rep.* 10:7905
- Liu H. 2009. Integrated modeling of insect flight: from morphology, kinematics to aerodynamics. *J. Comput. Phys.* 228:439–59
- Liu H. 2020. Simulation-based insect-inspired flight systems. *Curr. Opin. Insect Sci.* 42:105–9
- Liu H, Aono H. 2009. Size effects on insect hovering aerodynamics: an integrated computational study. *Bioinspiration Biomim.* 4:015002
- Liu H, Ellington CP, Kawachi K, van den Berg C, Willmott AP. 1998. A computational fluid dynamic study of hawkmoth hovering. *J. Exp. Biol.* 201:461–77
- Liu H, Nakata T, Li G, Kolomenskiy D. 2017. Unsteady bio-fluid dynamics in swimming and flying. *Acta Mech. Sin.* 33:663–84
- Liu H, Ravi S, Kolomenskiy D, Tanaka H. 2016. Biomechanics and biomimetics in insect-inspired flight systems. *Philos. Trans. R. Soc. B* 371:20150390
- Liu T, Kuykendoll K, Rhew R, Jones S. 2006. Avian wing geometry and kinematics. *ALAA J.* 44:954–63
- Lu Y, Shen GX, Lai GJ. 2006. Dual leading-edge vortices on flapping wings. *J. Exp. Biol.* 209:5005–16
- Lyu YZ, Zhu HJ, Sun M. 2019. Aerodynamic forces and vortical structures of a flapping wing at very low Reynolds numbers. *Phys. Fluids* 31:041901
- Maxworthy T. 2007. The formation and maintenance of a leading-edge vortex during the forward motion of an animal wing. *J. Fluid Mech.* 587:471–75
- Maybury WJ, Rayner JMV, Coudrick LB. 2001. Lift generation by the avian tail. *Proc. R. Soc. B* 268:1443–48
- Nakata T, Liu H. 2012a. Aerodynamic performance of a hovering hawkmoth with flexible wings: a computational approach. *Proc. R. Soc. B* 279:722–31
- Nakata T, Liu H. 2012b. A fluid–structure interaction model of insect flight with flexible wings. *J. Comput. Phys.* 228:439–59
- Nakata T, Liu H, Bomphrey R. 2015. A CFD-informed quasi-steady model of flapping-wing aerodynamics. *J. Fluid Mech.* 783:323–43
- Miller LA, Peskin CS. 2009. Flexible clap and fling in tiny insect flight. *J. Exp. Biol.* 212:3076–90
- Muijres FT, Johansson LC, Barfield R, Wolf M, Spedding GR, Hedenström A. 2008. Leading-edge vortex improves lift in slow-flying bats. *Science* 319:1250–53
- Muijres FT, Johansson LC, Winter Y, Hedenström A. 2011. Comparative aerodynamic performance of flapping flight in two bat species using time-resolved wake visualization. *J. R. Soc. Interface* 8:1418–28
- Muir RE, Arredondo-Galeana A, Viola IM. 2017. The leading-edge vortex of swift wing-shaped delta wings. *R. Soc. Open Sci.* 4:170077
- Nachtigall W, Wieser J. 1966. Profilmessungen am Taubenflügel. *Z. Vgl. Physiol.* 52:333–46
- Norberg UM, Winter Y. 2006. Wing beat kinematics of a nectar-feeding bat, *Glossophaga soricina*, flying at different flight speeds and Strouhal numbers. *J. Exp. Biol.* 209:3887–97
- Ozen CA, Rockwell D. 2012. Three-dimensional vortex structure on a rotating wing. *J. Fluid Mech.* 707:541–50
- Pennycuik CJ, Heine CE, Kirkpatrick SJ, Fuller MR. 1992. The profile drag of a hawk's wing, measured by wake sampling in a wind tunnel. *J. Exp. Biol.* 165:1–19
- Pesavento U, Wang ZJ. 2004. Falling paper: Navier-Stokes solutions, model of fluid forces, and center of mass elevation. *Phys. Rev. Lett.* 93:144501
- Phillips N, Knowles K, Bomphrey RJ. 2015. The effect of aspect ratio on the leading-edge vortex over an insect-like flapping wing. *Bioinspiration Biomim.* 10:056020
- Portugal SJ, Hubel TY, Fritz J, Heese S, Trobe D, et al. 2014. Upwash exploitation and down-wash avoidance by flap phasing in ibis formation flight. *Nature* 505:399–404
- Ramanarivo S, Godoy-Diana R, Thiria B. 2011. Rather than resonance, flapping wing flyers may play on aerodynamics to improve performance. *PNAS* 108:5964–69
- Riskin DK, Willis DJ, Iriarte-Diaz J, Hedrick TL, Kostandov M, et al. 2008. Quantifying the complexity of bat wing kinematics. *J. Theor. Biol.* 254:604–15
- Rosén M, Spedding GR, Hedenström A. 2004. The relationship between wingbeat kinematics and vortex wake of a thrush nightingale. *J. Exp. Biol.* 207:4255–68

- Rosén M, Spedding GR, Hedenström A. 2007. Wake structure and wingbeat kinematics of a house-martin *Delichon urbica*. *J. R. Soc. Interface* 4:659–68
- Sadier A, Urban DJ, Anthwal N, Howenstine AO, Sinha I, et al. 2020. Making a bat: the developmental basis of bat evolution. *Genet. Mol. Biol.* 43(1 Suppl. 2):e20190146
- Sane SP. 2003. The aerodynamics of insect flight. *J. Exp. Biol.* 206:4191–208
- Sane SP. 2016. Neurobiology and biomechanics of flight in miniature insects. *Curr. Opin. Neurobiol.* 41:158–66
- Sane SP, Dickinson MH. 2002. The aerodynamic effects of wing rotation and a revised quasi-steady model of flapping flight. *J. Exp. Biol.* 205:1087–96
- Santhanakrishnan A, Robinson AK, Jones S, Low AA, Gadi S, et al. 2014. Clap and fling mechanism with interacting porous wings in tiny insect flight. *J. Exp. Biol.* 217:3898–909
- Sedov LI. 1965. Mathematical methods for constructing new models of continuous media. *Russ. Math. Surv.* 20:123
- Shyy W, Aono H, Chimakurthi SK, Trizila P, Kang C-K, et al. 2010. Recent progress in flapping wing aerodynamics and aeroelasticity. *Prog. Aeronaut. Sci.* 46:284–327
- Shyy W, Trizila P, Kang C-K, Aono H. 2009. Can tip vortices enhance lift of a flapping wing? *ALAA J.* 47:289–93
- Sims TW, Palazotto AN, Norris AG. 2010. A structural dynamic analysis of a *Manduca sexta* forewing. *Int. J. Micro Air Veh.* 2:119–40
- Song JL, Cheney JA, Bomphrey RJ, Usherwood JR. 2022. Virtual manipulation of tail postures of a gliding barn owl (*Tyto alba*) demonstrates drag minimization when gliding. *J. R. Soc. Interface* 19:20210710
- Song JL, Luo HX, Hedrick TL. 2014. Three-dimensional flow and lift characteristics of a hovering ruby-throated hummingbird. *J. R. Soc. Interface* 11:20140541
- Spedding GR, Hedenström A, Rosen M. 2003a. Quantitative studies of the wakes of freely flying birds in a low-turbulence wind tunnel. *Exp. Fluids* 34:291–303
- Spedding GR, Rosen M, Hedenström A. 2003b. A family of vortex wakes generated by a thrush nightingale in free flight in a wind tunnel over its entire natural range of flight speeds. *J. Exp. Biol.* 206:2313–44
- Sridhar M, Kang C-K. 2015. Aerodynamic performance of two-dimensional, chordwise flexible flapping wings at fruit fly scale in hover flight. *Bioinspiration Biomim.* 10:036007
- Srygley RB, Thomas ALR. 2002. Unconventional lift-generating mechanisms in free-flying butterflies. *Nature* 420:660–64
- Sun M, Tang J. 2002. Unsteady aerodynamic force generation by a model fruit fly wing in flapping motion. *J. Exp. Biol.* 205:55–70
- Sun M, Wu JH. 2003. Aerodynamic force generation and power requirements in forward flight in a fruit fly with modeled wing motion. *J. Exp. Biol.* 206:3065–83
- Sunada S, Zeng L, Kawachi K. 1998. The relationship between dragonfly wing structure and torsional deformation. *J. Theor. Biol.* 193:39–45
- Swartz SM, Konow N. 2015. Advances in the study of bat flight: the wing and the wind. *Can. J. Zool.* 93:977–90
- Thomas ALR, Taylor GK, Srygley RB, Nudds RL, Bomphrey RJ. 2004. Dragonfly flight: free-flight and tethered flow visualizations reveal a diverse array of unsteady lift-generating mechanisms, controlled primarily via angle of attack. *J. Exp. Biol.* 207:4299–323
- Tobalske BW. 2007. Biomechanics of bird flight. *J. Exp. Biol.* 210:3135–46
- Tong W, Wang S, Yang Y. 2022. Estimating forces from cross-sectional data in the wake of flows past a plate using theoretical and data-driven models. *Phys. Fluids* 34:111905
- Tong W, Yang Y, Wang S. 2021. Estimating thrust from shedding vortex surfaces in the wake of a flapping plate. *J. Fluid Mech.* 920:A10
- Usherwood JR, Cheney JA, Song J, Windsor SP, Stevenson JPJ, et al. 2020. High aerodynamic lift from the tail reduces drag in gliding raptors. *J. Exp. Biol.* 223:jeb214809
- van Den Berg C, Ellington CP. 1997. The three-dimensional leading-edge vortex of a hovering model hawk moth. *Philos. Trans. R. Soc. B* 352:329–40
- van Veen WG, Van Leeuwen JL, Muijres FT. 2019. A chordwise offset of the wing-pitch axis enhances rotational aerodynamic forces on insect wings: a numerical study. *J. R. Soc. Interface* 16:20190118
- Vanella M, Fitzgerald T, Preidikman S, Balara E, Balachandran B. 2009. Influence of flexibility on the aerodynamic performance of a hovering wing. *J. Exp. Biol.* 212:95–105

- Videler JJ, Stamhuis EJ, Povel GDE. 2004. Leading-edge vortex lifts swifts. *Science* 306:1960–62
- Viswanath K, Nagendra K, Tafti D. 2014. *Climbing flight of a fruit bat deconstructed*. Paper presented at 52nd AIAA Aerospace Science Meeting, Washington, DC, AIAA Pap. 2014-0220
- Wakeling JM, Ellington CP. 1997. Dragonfly flight. II. Velocities, accelerations, and kinematics of flapping flight. *J. Exp. Biol.* 200:557–82
- Wang C, Liu Y, Xu D, Wang S. 2022. Aerodynamic performance of a bio-inspired flapping wing with local sweep morphing. *Phys. Fluids* 34:051903
- Wang Q, Goosen JFL, Van Keulen F. 2016. A predictive quasi-steady model of aerodynamic loads on flapping wings. *J. Fluid Mech.* 800:688–719
- Wang S, He G, Liu T. 2019. Estimating lift from wake velocity data in flapping flight. *J. Fluid Mech.* 868:501–37
- Wang S, Zhang X, He G, Liu T. 2013. A lift formula applied to low-Reynolds-number unsteady flows. *Phys. Fluids* 25:093605
- Wang S, Zhang X, He G, Liu T. 2014. Lift enhancement by dynamically changing wingspan in forward flapping flight. *Phys. Fluids* 26:061903
- Wang S, Zhang X, He G, Liu T. 2015a. Lift enhancement by bats' dynamically changing wingspan. *J. R. Soc. Interface* 12:20150821
- Wang S, Zhang X, He G, Liu T. 2015b. Numerical simulation of unsteady flows over a slow-flying bat. *Theor. Appl. Mech. Lett.* 5:5–8
- Wang ZJ. 2005. Dissecting insect flight. *Annu. Rev. Fluid Mech.* 37:183–210
- Warrick DR, Hedrick T, Fernández MJ, Tobalske B, Biewener A. 2012. Hummingbird flight. *Curr. Biol.* 22:R472–77
- Warrick DR, Tobalske BW, Powers DR. 2005. Aerodynamics of the hovering hummingbird. *Nature* 435:1094–97
- Weis-Fogh T. 1973. Quick estimates of flight fitness in hovering animals, including novel mechanism for lift production. *J. Exp. Biol.* 59:169–230
- Whitney JP, Wood RJ. 2010. Aeromechanics of passive rotation in flapping flight. *J. Fluid Mech.* 660:197–220
- Wolf T, Konrath R. 2015. Avian wing geometry and kinematics of a free-flying barn owl in flapping flight. *Exp. Fluids* 56:28
- Wolfinger M, Rockwell D. 2014. Flow structure on a rotating wing: effect of radius of gyration. *J. Fluid Mech.* 755:83–110
- Wolfinger M, Rockwell D. 2015. Transformation of flow structure on a rotating wing due to variation of radius of gyration. *Exp. Fluids* 56:137
- Wu T. 2011. Fish swimming and bird/insect flight. *Annu. Rev. Fluid Mech.* 43:25–58
- Xu R, Zhang X, Liu H. 2021. Effects of wing-to-body mass ratio on insect flapping flights. *Phys. Fluids* 33:021902
- Xue Y, Cai X, Liu H. 2022. Effects of wing–body interaction on hawkmoth aerodynamics and energetics at various flight velocities. *Phys. Fluids* 34:051915
- Yao J, Yeo KS. 2020. Forward flight and sideslip manoeuvre of a model hawk moth. *J. Fluid Mech.* 896:A22
- Yin B, Luo H. 2010. Effect of wing inertia on hovering performance of flexible flapping wings. *Phys. Fluids* 22:111902
- Young J, Walker SM, Bomphrey RJ, Taylor GK, Thomas ALR. 2009. Details of insect wing design and deformation enhance aerodynamic function and flight efficiency. *Science* 325:1549–52
- Zheng L, Hedrick TL, Mittal R. 2012. Time-varying wing-twist improves aerodynamic efficiency of forward flight in butterflies. *PLOS ONE* 8:e53060